1. Introduction

In a fluid confined to a plane layer and heated from below, convection can occur in rolls, in square, rectangular or hexagonal cells, or in more complicated or even turbulent spatial configurations. Even with a given spatial structure, the temporal behaviour can be steady, oscillatory, quasiperiodic or chaotic. As the controlling parameters (for example, the Rayleigh number, proportional to the imposed temperature gradient) vary, there are transitions (bifurcations) where one type of convective behaviour loses stability to another. This paper is concerned with the analysis of the temporal behaviour of two-dimensional double convection: roll convection in the presence of a stabilizing solute gradient, a magnetic field or in a rotating layer.

The numerical solution of the partial differential equations (PDEs) that govern double convection reveals a rich variety of spatial and temporal structure. For example, the PDEs governing two-dimensional thermosolutal convection have chaotic solutions created after a period-doubling cascade (Knobloch, Moore, Toomre & Weiss 1986). However, the results of such numerical studies are often difficult to interpret, especially if more than one of the physical parameters specifying the problem is varied in order to study a particular bifurcation. For this reason, low-order models are essential if the origins of the chaotic behaviour are to be understood.

Such low-order models are typically derived by Galërkin truncations: the spatial structure is limited to a finite number of modes, and the variables that describe the state of the fluid are expanded in terms of these modes. These expansions are substituted into the PDEs, resulting in a set of coupled ordinary differential equations (ODEs) for the amplitudes of the modes. If this set of ODEs is to model the physical problem correctly, the modes that have been discarded must not play an important role in the behaviour of the system. The celebrated Lorenz (1963) equations are an example of a model of convection derived in this way. This third-order set of ODEs was first derived for Bénard convection in rolls, and aroused much interest as it has chaotic solutions for some parameter values. The Lorenz system correctly describes the transition to steady convection but, viewed solely as a model of convection, it is deficient on two counts: it predicts that the bifurcation from steady convection to oscillatory convection is subcritical and that there is chaotic convection. Numerical solutions of the full PDEs reveal that the bifurcation to oscillatory convection is supercritical, and that chaotic solutions do not appear in the PDEs (Moore & Weiss 1973). The inconsistency between the predictions of the Lorenz model and the observed behaviour of the PDEs arises because the convecting system is not described accurately by three modes at the high Rayleigh numbers where the model has chaotic solutions. Indeed, the chaos predicted by the three mode Lorenz model disappears as more modes are included in the truncation (Curry, Herring, Loncaric & Orszag 1984).

Restricting the controlling parameters to a small region of parameter space near the initial bifurcation from the trivial solution introduces a small parameter

that we may use to scale the amplitudes of the various modes. The resulting amplitude equations are asymptotically exact if the corrections from the discarded modes can be made as small as we wish by remaining close enough to the initial bifurcation; solutions to asymptotically exact equations will provide asymptotically correct solutions to the full PDEs.

The key issue is to establish, for a truncation of a given set of PDEs, that the modes that have been discarded are of negligible amplitude. This is clear, for example, in the familiar case of Bénard convection in a square box just above the onset of convection: if we let $R = R_{\mathrm{C}}(1 + \epsilon^2\mu)$, where R is the Rayleigh number, R_{C} is the Rayleigh number at the onset of convection, μ is an unfolding parameter and ϵ is a small parameter, then the amplitude of the single-roll mode will be order ϵ, and all higher order modes will have amplitude order ϵ^2 or smaller, and can be neglected. In this case, the ODE governing the evolution of a, the amplitude of the single-roll mode, will be:

$$\dot{a} = \mu a - Ma^3 + \mathcal{O}(\epsilon), \tag{1}$$

where M is a (positive) constant. This equation is an asymptotically exact description of the PDEs for roll convection in a layer of Boussinesq fluid, in the limit of $\epsilon \to 0$. For μ less than zero, the trivial solution $a = 0$ is stable; as μ increases through zero, there is a pitchfork bifurcation to steady convection.

In thermosolutal or magnetoconvection, the competition between the destabilizing temperature gradient and the stabilizing solute gradient or magnetic field can lead to oscillatory convection, if the solute gradient or magnetic field are big enough. If they are not, then a sufficiently large temperature gradient will lead to steady convection. In convection in a layer of fluid rotating about a vertical axis, the competition between buoyancy and Coriolis forces can lead to similar behaviour. There is thus a bi-critical point "C" where the type of motion seen at the onset of convection changes from steady to oscillatory convection (see Figure 1). At this point C, the system has two zero eigenvalues, so C is a codimension-two Bogdanov bifurcation point. Within an ϵ^2-neighbourhood of this point C, thermosolutal convection has small-amplitude (order ϵ) solutions that are described accurately by the second-order Van der Pol–Duffing equation:

$$\ddot{a} - Ma^3 + \lambda a = \epsilon\kappa\dot{a} + \epsilon N a^2\dot{a} + \mathcal{O}(\epsilon^2) \tag{2}$$

(Coullet & Spiegel 1983), where a is the amplitude of the lowest-order mode of the stream-function, the dot stands for the derivative with respect to a scaled time, κ and λ are unfolding parameters, which are zero at the point C, and M and N are constants. The contributions of the higher-order modes enter at order ϵ^2 in equation (2) and can be made as small as we wish by going close enough to the point C. Equation (2) can also be derived for convection in a rotating layer of fluid

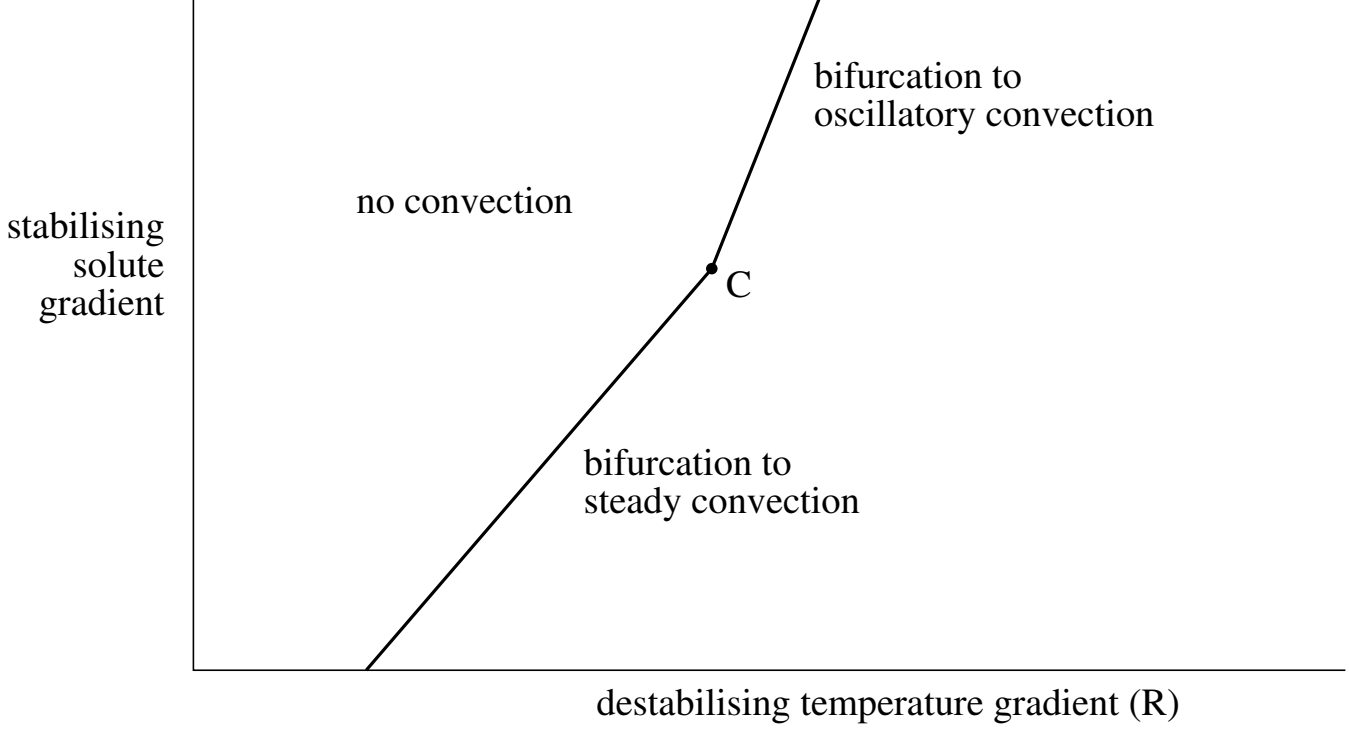

Figure 1. *Unfolding diagram showing the type of motion seen at the onset of convection as the temperature gradient is increased, in the case of thermosolutal convection. At the codimension-two point C, the initial Hopf and pitchfork bifurcations are coincident. (After Huppert & Moore 1976.)*

(Guckenheimer & Knobloch 1983); Knobloch & Proctor (1981) found analytic expressions for weakly nonlinear oscillatory thermosolutal convection and convection in a vertical magnetic field using effectively the same equation.

Equation (2) can be derived from two fifth-order sets of ODEs for thermosolutal convection (Veronis 1965) and for convection in a vertical magnetic field (Knobloch, Weiss & Da Costa 1981). There are related fifth-order models for convection in a horizontal magnetic field (Arter 1983) and for convection in a rotating layer of fluid (Veronis 1966). These models have several features in common: they are descriptions of double convection for Boussinesq fluids confined to rolls of fixed width with mathematically convenient boundary conditions, and were derived by truncating Galërkin representations of the relevant system of PDEs. The only modes that are included are those that are necessary for consistent and nontrivial models. The models all have a codimension-two point C where the linearised problem has two zero eigenvalues. Near the point C, they can all be reduced to the asymptotically exact second-order model (2) (Knobloch & Proctor 1981, Knobloch 1986a, Guckenheimer & Knobloch 1983).

By considering the limit of tall, thin rolls, Proctor & Weiss (1990) derived an asymptotically exact fourth-order set of ODEs describing small-amplitude convection near the codimension-two point C for thermosolutal convection, and simplified

the model to third-order in the limit of small solutal diffusivity:

$$\begin{aligned} \ddot{a} + \lambda a &= \kappa \dot{a} + ac, \\ \dot{c} &= -c + a^2. \end{aligned} \tag{3}$$

These equations have chaotic solutions associated with heteroclinic trajectories between saddle-foci that satisfy Shil'nikov's (1965; see also Glendinning & Sparrow 1984) criterion. The same equations are obtained by taking the two limits in opposite order: solutal diffusivity going to zero yields the Lorenz equations, which are only an asymptotically exact model in the limit of small-amplitude convection near the point C, where they reduce to equations (2); then, in the limit of tall, thin rolls, equations (3) are recovered (Knobloch, Proctor & Weiss 1991). Although the model is asymptotically exact only for convection in tall, thin rolls and with small solutal diffusivity, it agrees qualitatively with the numerical solutions of the PDEs for two-dimensional thermosolutal convection in rolls with aspect ratio of order one (Knobloch *et al.* 1986). In a related study of triple convection (thermosolutal convection in a layer of fluid rotating about a vertical axis), Arnéodo, Coullet & Spiegel (1982; 1985) presented an asymptotically exact third-order model that has chaotic solutions associated with homoclinic or heteroclinic trajectories between saddle-foci that satisfy Shil'nikov's criterion for the existence of stable chaos, and that is in quantitative agreement with the PDEs describing the full problem (Arnéodo & Thual 1985).

In section 2, I assemble four sets of fifth-order ODEs that have been derived as Galërkin truncations of four double-diffusive problems: thermosolutal convection (case T), magnetoconvection in imposed vertical (case V) and horizontal (case H) magnetic fields, and convection in a fluid rotating uniformly about a vertical axis (case R). In section 3, I derive all possible asymptotically exact low-order models for each case. The model for thermosolutal convection and for convection in an imposed horizontal magnetic field in the limits on tall, thin rolls and small diffusivities is equations (3); this derivation of an asymptotically exact model for horizontal magnetoconvection, along with the results of Proctor & Weiss (1990), demonstrate the existence of chaos in magnetoconvection. For convection in an imposed vertical magnetic field and for convection in a rotating layer, with the motion confined to tall, thin rolls, the model equations are:

$$\begin{aligned} \ddot{a} + \lambda a &= \kappa \dot{a} - ac, \\ \dot{c} &= -c + a^2, \end{aligned} \tag{4}$$

which differ from equations (3) only in the sign of the nonlinearity in the first equation. This difference alters the behaviour of the nonlinear solutions completely.

A detailed study of equations (4) is presented by Rucklidge (1991); in section 4, I show that chaotic solutions are associated with homoclinic connections to a saddle, in the same manner as the chaotic solutions of the Lorenz equations.

This type of chaotic behaviour contrasts with the chaos seen in equations (3), associated with heteroclinic connections between saddle-foci that satisfy Shil'nikov's criterion for the existence of stable chaos. The existence of chaos in the model equations (4) establishes the existence of temporal chaos in the PDEs governing convection confined to tall, thin rolls in an imposed vertical magnetic field or in a rotating layer.

2. Reduction to a fifth-order set of ODEs

Four problems are considered: thermosolutal convection (case T), magneto-convection with an imposed vertical (case V) or horizontal (case H) magnetic field, and convection in a fluid layer rotating uniformly about a vertical axis (case R). Although the details of the interactions differ in each case, there is enough similarity that all four may be considered at once. Since these are model problems, intended to illustrate the type of behaviour that may be observed, everything will be kept as simple as possible: the fluids under consideration are conducting Boussinesq fluids, and the boundary conditions are chosen so that the eigenfunctions of the linearised problem are harmonic. Only two-dimensional convection (rolls) will be considered, with the motion confined to a box of height h in the z-direction and width Lh in the x-direction. The fluid is heated from below, and, in the case of thermosolutal convection, salted from below. Magnetic buoyancy will be neglected. In case R, we shall use co-rotating coordinates.

2.1. The PDEs

We shall use the standard vorticity formulation for the PDEs governing these problems (Da Costa, Knobloch & Weiss 1981; Knobloch, Weiss & Da Costa 1981; Arter 1983; Guckenheimer & Knobloch 1983). The state of the fluid is described by the stream function Ψ, the vorticity ω and the temperature T. The second quantity in these double convection problems will be denoted by S in all cases, in order to bring out the similarity between the problems. In case T, S is the concentration of the solute; in cases V and H, S is the magnetic flux function; and in case R, S is the y-component of the velocity (which is zero except in case R). Likewise, ζ will represent the relative diffusivity of the quantity S in all four cases, so in case T, ζ is the ratio of the solutal diffusivity (κ_S) to the heat diffusivity (κ); in cases V and H, ζ is the ratio of the magnetic diffusivity (η) to the heat diffusivity; and in case R, ζ is equal to the Prandtl number σ, the ratio of the viscous diffusivity (ν) to the heat diffusivity.

The problem has a static solution, in which there is no motion ($\Psi = 0$, and $S = 0$ in case R), the temperature, and solute concentration in case T, have relaxed to linear profiles across the box, and the magnetic field in cases V and H is uniform. The linear temperature profile of this trivial solution is $T_0 = 1 - z$, and we will expand about it: $T = T_0 + \theta$. Similarly, we expand S about its static profile S_0:

Case	$f_1(\Sigma)$	$f_2(\Psi)$	Q	Q_S	C_4	C_5
T	$\sigma Q\dfrac{\partial\Sigma}{\partial x}$	$\dfrac{\partial\Psi}{\partial x}$	$\dfrac{g\beta h^3}{\kappa\nu}\Delta S$	$\dfrac{64\pi^4\zeta}{\varpi^2(4-\varpi)}$	$\dfrac{\sqrt{2\varpi}}{\pi}$	$-\dfrac{1}{\pi}$
V	$-\sigma\zeta Q\left(\dfrac{\partial\nabla^2\Sigma}{\partial z}+\mathrm{J}\left(\Sigma,\nabla^2\Sigma\right)\right)$	$\dfrac{\partial\Psi}{\partial z}$	$\dfrac{h^2}{\mu_0\rho_0\eta\nu}\mathbf{B}_0^2$	$\dfrac{16\pi^2}{\varpi^2}$	$\dfrac{\varpi\sqrt{2}}{\pi\sqrt{4-\varpi}}$	$\dfrac{\sqrt{\varpi}}{\pi\sqrt{4-\varpi}}$
H	$-\sigma\zeta Q\left(\dfrac{\partial\nabla^2\Sigma}{\partial x}+\mathrm{J}\left(\Sigma,\nabla^2\Sigma\right)\right)$	$\dfrac{\partial\Psi}{\partial x}$	$\dfrac{h^2}{\mu_0\rho_0\eta\nu}\mathbf{B}_0^2$	$\dfrac{16\pi^2}{\varpi(4-\varpi)}$	$\dfrac{\sqrt{2\varpi}}{\pi}$	$-\dfrac{1}{\pi}$
R	$\sigma Q\dfrac{\partial\Sigma}{\partial z}$	$\sigma Q\dfrac{\partial\Psi}{\partial z}$	$\dfrac{2h^2}{\nu}\Omega$	$\dfrac{8\pi^2}{\varpi\sqrt{\varpi}}$	$\dfrac{\varpi\sigma Q\sqrt{2}}{\pi\sqrt{4-\varpi}}$	$\dfrac{\sigma Q\sqrt{\varpi}}{\pi\sqrt{4-\varpi}}$

Table 1. *Definitions of quantities that are different in each case.*

$S = S_0 + \Sigma$, and obtain the PDEs:

$$\nabla^2\Psi = -\omega, \tag{5}$$

$$\frac{\partial\omega}{\partial t} + \mathrm{J}\left(\Psi,\omega\right) = \sigma\nabla^2\omega - \sigma R\frac{\partial\theta}{\partial x} + f_1(\Sigma), \tag{6}$$

$$\frac{\partial\theta}{\partial t} + \mathrm{J}\left(\Psi,\theta\right) = \nabla^2\theta + \frac{\partial\Psi}{\partial x}, \tag{7}$$

$$\frac{\partial\Sigma}{\partial t} + \mathrm{J}\left(\Psi,\Sigma\right) = \zeta\nabla^2\Sigma + f_2(\Psi), \tag{8}$$

where the Jacobian J is defined by $\mathrm{J}(f,g) = \partial(f,g)/\partial(x,z)$, the Rayleigh number $R = g\alpha h^3\Delta T/\kappa\nu$, and Q is the solutal Rayleigh number in case T, the Chandrasekhar number in cases V and H and the square root of the Taylor number in case R. The quantities that vary between the four cases are defined in Table 1. Throughout, g is the acceleration due to gravity (acting in the negative z direction), α and β are the thermal and solutal expansion coefficients, ρ_0 is the reference density, μ_0 is the magnetic permeability of the fluid, ΔT and ΔS are the imposed temperature and solute concentration differences, $\mathbf{B}_0$ is the imposed magnetic field, and Ω is the uniform rotation rate. The PDEs (5)–(8) are nondimensionalised by scaling the time t by the thermal conduction time κ/h^2 and distance by the height h of the box.

Equations (6)–(8) are all in advection-diffusion form: vorticity, heat, solute, and magnetic flux are all transported by the fluid motion, and all diffuse. The vorticity equation (6) has additional forcing terms that describe how the fluid motion is affected by the other variables: temperature gradients and solute gradients give

rise to buoyancy forces, a magnetic field in a conducting fluid gives rise to a Lorentz force, and there is a Coriolis force in the case of rotation.

The boundary conditions are chosen so that the linearised problem has sinusoidal eigenfunctions, which is necessary if the nonlinear analysis is to be tractable. With other choices of boundary condition, we would expect to obtain essentially the same low-order models but with different coefficients, which would have to be calculated numerically. The boundary conditions are: stress-free boundaries, so $\Psi = \omega = 0$ on the boundaries; fixed temperature ($\theta = 0$) on the top and bottom walls and no heat flux ($\partial\theta/\partial x = 0$) across the side walls. In case T, we impose fixed solute concentration ($\Sigma = 0$) on the top and bottom walls and no solute flux ($\partial\Sigma/\partial x = 0$) across the side walls. In cases V and H, we require that the magnetic field at the boundary of the box be parallel to the imposed field; this translates as $\partial\Sigma/\partial z = 0$ ($\Sigma = 0$) on the top and bottom walls and $\Sigma = 0$ ($\partial\Sigma/\partial x = 0$) on the side walls in case V (H). In case R, the stress-free condition requires that $\partial\Sigma/\partial z = 0$ on the top and bottom walls and $\Sigma = 0$ on the side walls.

2.2. Expansion in a harmonic series

The variables ω, Ψ, θ and Σ may be expanded as sums over the appropriate linear eigenfunctions, determined by the boundary conditions. For example, we may write

$$\Psi = \sum_{m=1}^{\infty}\sum_{n=1}^{\infty} a_{m,n}(t)\sin\frac{m\pi x}{L}\sin n\pi z.$$

The variables θ and Σ may be represented by similar sums. If we consider only weakly nonlinear convection, only a few terms in each sum are required to describe the motion of the fluid accurately. Indeed, numerical computations of Rayleigh–Bénard convection suggest that the linear single-roll eigenfunction approximates the true nonlinear eigenfunction closely for R near its critical value (Deane & Sirovich 1991). For the linear analysis, only the first term in each sum is required, and each harmonic will act independently. The nonlinearities in the governing PDEs will cause the harmonics to interact: the first nonlinear effects are the distortions of θ and Σ, which are represented by including appropriate second-order harmonics. The simplest consistent representation is:

$$\Psi = C_1 a(t^*)\sin(\pi x/L)\sin\pi z, \tag{9}$$

$$\theta = C_2 b(t^*)\cos(\pi x/L)\sin\pi z + C_3 c(t^*)\sin 2\pi z, \tag{10}$$

$$\Sigma = \begin{cases} C_4 d(t^*)\cos(\pi x/L)\sin\pi z + C_5 e(t^*)\sin 2\pi z & \text{cases T and H,} \\ C_4 d(t^*)\sin(\pi x/L)\cos\pi z + C_5 e(t^*)\sin(2\pi x/L) & \text{cases V and R,} \end{cases} \tag{11}$$

where t^* is a scaled time: $t^* = C_6 t$, and C_1 to C_6 are constants chosen to simplify the final equations. Four of the six constants are the same in all cases:

$$C_1 = 4\sqrt{2/(4-\varpi)}, \qquad C_2 = \sqrt{2\varpi}/\pi, \qquad C_3 = -1/\pi, \qquad C_6 = \varpi/4\pi^2,$$

where the geometrical parameter $\varpi = 4L^2/(1+L^2)$; the remaining two constants are defined in Table 1. Note that $\varpi = 0$ in the limit of tall, thin rolls, and $\varpi = 4$ in the limit of short, wide rolls. It is also convenient to scale R and Q:

$$R = \frac{64\pi^4}{\varpi^2(4-\varpi)} r \qquad \text{and} \qquad Q = \begin{cases} Q_S\, q & \text{cases T, V and H,} \\ Q_S\, \sqrt{q} & \text{case R,} \end{cases}$$

where Q_S is defined in Table 1. The scalings of Q in cases T and R are non-standard, but are chosen for later convenience. At this point, we make no claim that the particular forms chosen for Ψ, θ and Σ are faithful representations; this is considered in more detail in section 3. However, the particular choice of sines and cosines in the expansion of Ψ, θ and Σ is consistent, in that no other low-order harmonics are generated by the nonlinear terms in the PDEs.

We substitute the expansion (9)–(11) into the PDEs (5)–(8) and equate the coefficients of the low-order eigenfunctions, resulting in five ODEs for the amplitudes a–e (Veronis 1965 and 1966; Knobloch, Weiss & Da Costa 1981; Arter 1983). By introducing

$$\gamma = \begin{cases} 0 & \text{cases T and R,} \\ 3-\varpi & \text{case V,} \\ \varpi - 1 & \text{case H,} \end{cases} \qquad \text{and} \qquad \delta = \begin{cases} \varpi & \text{cases T and H,} \\ 4-\varpi & \text{cases V and R,} \end{cases}$$

the amplitude equations may be written:

$$\begin{aligned} \dot{a} &= -\sigma a + \sigma r b - \sigma\zeta q d - \sigma\zeta q\gamma e d, \\ \dot{b} &= a - b - ac, \\ \dot{c} &= -\varpi c + \varpi ab, \\ \dot{d} &= a - \zeta d - ae, \\ \dot{e} &= -\zeta\delta e + \varpi ad. \end{aligned} \tag{12}$$

The dot stands for the derivative with respect to the scaled time t^*. The nonlinearity in the $\dot{a}$ equation in (12) is a result of the Lorentz force in cases V and H, and does not appear in cases T and R, when γ vanishes.

As discussed in the Introduction, this fifth-order set of ODEs (12) is not an asymptotically exact approximation to the full PDEs since we have not explicitly forced the amplitude of the motion to be small by restricting ourselves to a small neighbourhood of the codimension-two point C. In the next section, we will choose the parameters and scale the dependent variables so as to obtain sets of ODEs that are asymptotically exact approximations.

3. Reduction to asymptotically exact model equations

The eigenvalue equation for the equation (12) linearised about the trivial fixed point $a = b = c = d = e = 0$ has a double zero at the codimension-two bifurcation

point C: $(r, q) = (r_C, q_C)$, where $r_C = (\sigma + \zeta)/\sigma(1 - \zeta)$ and $q_C = \zeta(1 + \sigma)/\sigma(1 - \zeta)$. We must have $\zeta < 1$ in order to allow oscillatory convection. We will expand about the point (r_C, q_C): $r = r_C(1 + \mu)$ and $q = q_C(1 + \nu)$.

Of the five eigenvalues at the codimension-two bifurcation point C, the first two are zero, and

$$s_3 = -\varpi, \qquad s_4 = -\zeta\delta, \qquad s_5 = -(1 + \sigma + \zeta).$$

It is the total number of eigenvalues with zero real part that determines the dimension of the resulting set of ODEs, since all modes with eigenvalues with negative real part will be slaved to the marginal modes. Thus we will in effect be performing a centre manifold reduction (Guckenheimer & Holmes 1986). There are two zero eigenvalues at the point C, and there is a possibility of up to two more: in the limit of tall, thin rolls, s_3 is zero; in the limit of small ζ, or in the limit of tall, thin rolls in cases T and H and short, wide rolls in cases V and R, s_4 is zero. All possible limits will be considered.

The point of considering limiting situations in deriving low-order models is that increasing the number of zero eigenvalues increases the codimension of the bifurcation point and thus the order of the final ODEs that govern the dynamics on the centre manifold, allowing more complicated behaviour. It is typically found that the behaviour of a system near a high codimension bifurcation point provides a reliable guide to the behaviour observed in fairly extensive regions of parameter space about the bifurcation point. In conjunction with this, introducing a small parameter may force us to scale the unfolding parameters and the dependent variables in such a way that we are always close to the multiple bifurcation point (that is, μ and ν are small compared to 1), and the deviations from the trivial solution are small (that is, Ψ, θ and Σ are small compared to 1), so the solutions to the amplitude equations will yield, to within a small correction, solutions to the original PDEs. Thus the ODEs are an asymptotically exact approximation to the PDEs when

$$C_1 a \ll 1, \qquad C_3 c \ll C_2 b \ll 1, \qquad C_5 e \ll C_4 d \ll 1, \tag{13}$$

and

$$\mu \ll 1, \qquad \nu \ll 1. \tag{14}$$

When these conditions (13) and (14) hold, the amplitude of the convective motion is weak, and the contributions to the amplitude equations from the higher order modes is weaker still.

3.1. Small-amplitude motion

The same approach will be used in this and the next section, following Knobloch & Proctor (1981): a small parameter (ζ, ϖ, δ or the amplitude of the motion) is chosen, a slow time is introduced (scaled by this parameter), and the variables a to e are scaled. The appropriate variables, determined by the eigenvalues that

are large and negative, are eliminated by a sequence of substitutions that leaves those variables expressed as a power series in the small parameter. The unfolding parameters μ and ν are scaled in such a way as to bring several of the leading terms in the remaining equations to the same order. In the following derivations, (u, v, w, x, y) and (m, n, p, q, r) will be scaled versions of (a, b, c, d, e), and κ and λ will be scaled linear combinations of μ and ν. They will not necessarily have the same form in each derivation. Also, dots will refer to the derivative with respect to the newly-scaled time.

If none of s_3, s_4 or s_5 are small, then the only small parameter that may be introduced is the amplitude of the motion ϵ, which will be related to the distance from the multiple bifurcation point. Let

$$a = \epsilon u, \qquad b = \epsilon v, \qquad c = \epsilon^2 w, \qquad d = \epsilon x, \qquad e = \epsilon^2 y,$$

and scale time by a factor of $1/\epsilon$. The variables v, w, x and y may be eliminated in favour of u by a series of substitutions (Knobloch & Proctor 1981). The equation for $\dot{u}$ is expressed as a power series in ϵ: the first terms are

$$0 = \left(\frac{(\sigma + \zeta)\mu - \zeta(1 + \sigma)\nu}{1 - \zeta} \right) u - \epsilon \left(\frac{(\sigma + \zeta)\mu - (1 + \sigma)\nu}{1 - \zeta} \right) \dot{u} + \mathcal{O}(\epsilon^2).$$

Rescaling μ and ν by ϵ^2 will move the order 1 and order ϵ terms in this equation to order ϵ^2. This rescaling of μ and ν implies that we must be within an ϵ^2 neighbourhood of the codimension-two bifurcation point C; if we were not in this neighbourhood, then the resulting amplitude equation would be either $u = 0$ or $\dot{u} \propto u$. With μ and ν scaled, we obtain the Van der Pol–Duffing equation:

$$\ddot{u} - Mu^3 + \lambda u = \epsilon\kappa\dot{u} + \epsilon N u^2 \dot{u} + \mathcal{O}(\epsilon^2), \tag{15}$$

where

$$\mu = \epsilon^2 \left(\frac{\Delta}{\sigma + \zeta}\kappa + \lambda \right), \qquad \nu = \epsilon^2 \left(\frac{\Delta}{\zeta(1 + \sigma)}\kappa + \frac{1}{\zeta^2}\lambda \right),$$

$\Delta = 1 + \sigma + \zeta$, and M and N are complicated order 1 expressions involving σ, ζ and ϖ that can be set to ± 1 by rescaling u and t. It is necessary to retain the order ϵ terms in equation (15) to break the degeneracy of the bifurcation to oscillatory convection.

For Q below its critical value ($\nu < 0$), the instability sets in as steady convection, while if Q is above its critical value, the first instability is to oscillatory convection, with a second bifurcation to unstable steady convection. Using equation (15), we can draw bifurcation diagrams for the initial instabilities of the trivial (conducting) solution (Figure 2). In these diagrams, we consider a fixed Q above its critical value, and increase the temperature gradient, which corresponds to keeping $\nu > 0$ fixed and increasing μ, or taking a slice through the (κ, λ) plane with increasing κ and correspondingly decreasing λ. The signs of M and N for cases T, V, H

and R for various values of ϖ and ζ are shown in Table 2. The bifurcation to steady convection is subcritical if $M > 0$, and supercritical if $M < 0$; the bifurcation to oscillatory convection depends similarly on the sign of N.

3.2. Cases T and H

We can introduce a small parameter by considering the limit of small diffusivity ($\zeta \to 0$), the limit of tall, thin rolls ($\varpi \to 0$), or both. The limit of short, wide rolls does not introduce a relevant small parameter, as neither of the eigenvalues s_3 and s_4 are small in this limit. Proceeding first to the limit of small diffusivity, the appropriate scaling is

$$a = \zeta m, \qquad b = \zeta n, \qquad c = \zeta^2 p, \qquad d = q, \qquad e = r,$$

with time scaled by a factor of $1/\zeta$ from the original time. The variables n and p may be eliminated in favour of m by back-substitution. The final equations are:

$$\begin{aligned} \dot{m} &= (1+\lambda)m - (1+\kappa)q - \gamma(1+\kappa)qr, \\ \dot{q} &= m - q - mr, \\ \dot{r} &= -\varpi r + \varpi mq, \end{aligned} \tag{16}$$

where $\mu = \zeta(1+\sigma)\lambda/\sigma$ and $\nu = \kappa$. From the expression for ν, and from the lack of scaling of the variables d and e, it is clear that we are not necessarily near the codimension-two bifurcation point C, and that the amplitude of the motion need not be small (order ζ); this implies that equations (16) are not an asymptotically exact approximation to the full PDEs. If we were to insist that d and e were small, or that we were within a small neighbourhood of the point C, we would end up with a second-order set of ODEs. In case T ($\gamma = 0$), a simple rescaling will transform the equations (16) into the Lorenz equations, with negative Prandtl number (Knobloch, Proctor & Weiss 1991).

It is now possible to let ϖ be a second small parameter. The appropriate scaling in this situation is:

$$m = \varpi u, \qquad q = \varpi x, \qquad r = \varpi^2 y,$$

with time further scaled by a factor of $1/\varpi$. The variable x may now be eliminated in favour of u; the resulting set of ODEs is:

$$\begin{aligned} \ddot{u} + \lambda u &= \kappa\dot{u} + Suy, \\ \dot{y} &= -y + u^2, \end{aligned} \tag{17}$$

where $\mu = \zeta\varpi(1+\sigma)\kappa/\sigma - \zeta\varpi^2(1+\sigma)\lambda/\sigma$, $\nu = \varpi\kappa$ and $S = 1$ in case T and 2 in case H. Since conditions (13)–(14) are now satisfied, equations (17) are an asymptotically exact approximation to the full PDEs. By scaling the factor S to 1,

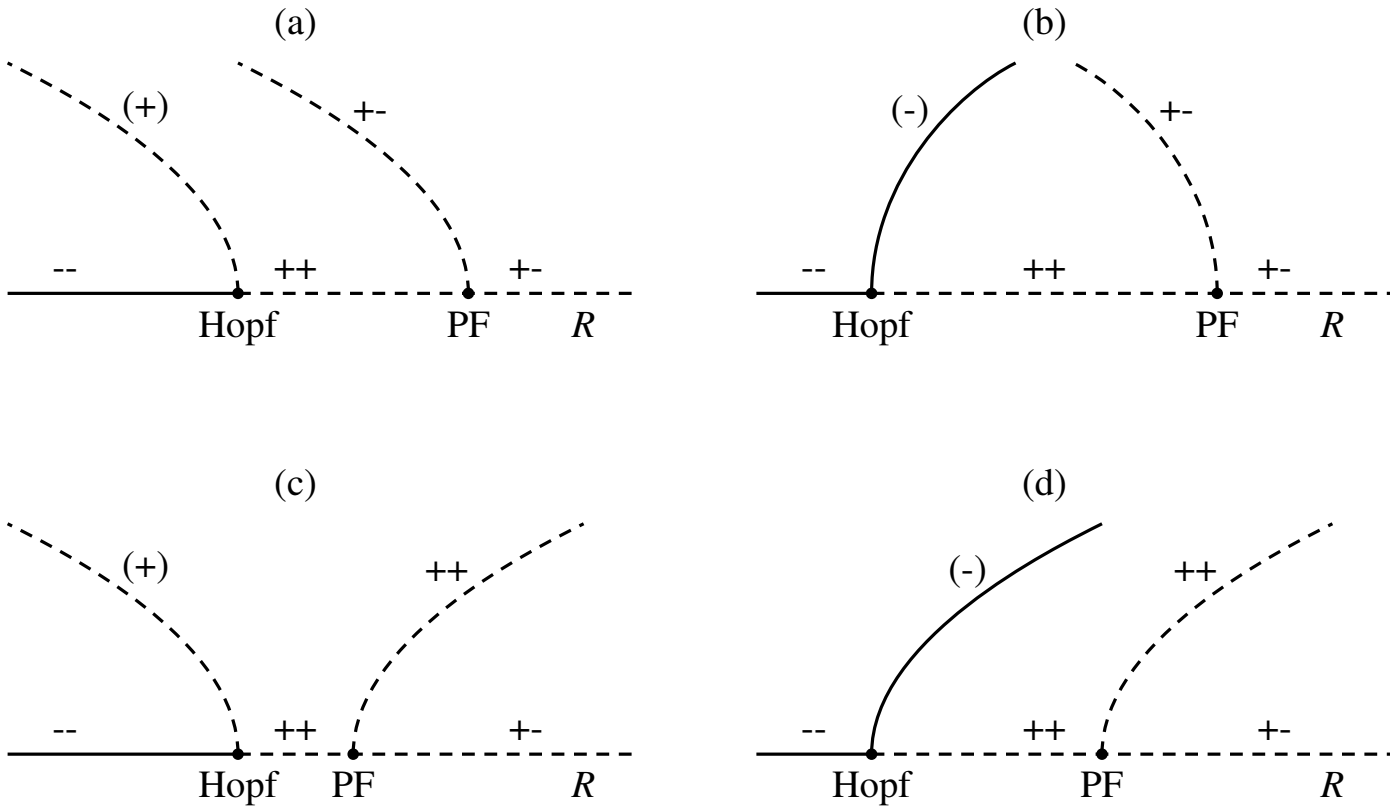

Figure 2. *Bifurcations from the trivial (conducting) solution. These schematic diagrams show the amplitude of the convecting solution on the vertical axis as a function of increasing Rayleigh number R, assuming that Q is above its critical value. The first bifurcation (left) is to oscillatory convection, and the second bifurcation (right) is to steady convection. (a) $M > 0$ and $N > 0$. (b) $M > 0$ and $N < 0$. (c) $M < 0$ and $N > 0$. (d) $M < 0$ and $N < 0$. Solid and dashed lines indicate stable and non-stable solutions respectively. The signs $+$ and $-$ indicate the signs of the real parts of the eigenvalues determining the stability of the solution: $--$ indicates a sink, $+-$ a saddle and $++$ a source; $(-)$ and $(+)$ indicate stable and unstable periodic orbits respectively. The filled circles represent local (pitchfork (PF) and Hopf) bifurcations.*

Case	Tall thin rolls (M, N)	Short wide rolls (M, N)	Small diffusivity (M, N)
T	$(+, -)$	—	$(+, -)$
V	$(-, +)$	$(+, -)$	$(\sim(\varpi - 2), -)$
H	$(+, -)$	—	$(\sim(2 - \varpi), -)$
R	$(-, +)$	$(+, -)$	$(+, -)$

Table 2. *The signs of M and N for cases T, V, H and R, in the limits of tall thin rolls, short wide rolls (cases V and R only) and small diffusivity.*

we recover the equations that Proctor & Weiss (1990) derived for case T in the limit of tall, thin rolls and small solutal diffusivity; the derivation for case H is new.

If we now return to the original fifth-order equations (12), and take the two limits in opposite order, we set

$$a = \varpi m, \qquad b = \varpi n, \qquad c = \varpi^2 p, \qquad d = \varpi q, \qquad e = \varpi^2 r,$$

and scale time by a factor of $1/\varpi$ from the original time. The variables n and q may be eliminated in favour of m, p and r, yielding the following equations:

$$\begin{aligned} \ddot{m} + \lambda m &= \kappa \dot{m} - Rmp + Smr, \\ \dot{p} &= -p + m^2, \\ \dot{r} &= -\zeta r + m^2/\zeta, \end{aligned} \tag{18}$$

where

$$\mu = \varpi \frac{\Delta}{\sigma + \zeta}\kappa - \varpi^2 \frac{\Delta}{\zeta(\sigma + \zeta)}\lambda, \qquad \nu = \varpi \frac{\Delta}{\zeta(1 + \sigma)}\kappa - \varpi^2 \frac{\Delta}{\zeta(1 + \sigma)}\lambda,$$

$$R = \frac{\zeta(\sigma + \zeta)}{\Delta(1 - \zeta)}, \qquad S = \begin{cases} \dfrac{\zeta^2(1 + \sigma)}{\Delta(1 - \zeta)} & \text{case T}, \\ 2\dfrac{\zeta^2(1 + \sigma)}{\Delta(1 - \zeta)} & \text{case H}. \end{cases}$$

Since conditions (13)–(14) are satisfied, equations (18) are an asymptotically exact approximation to the full PDEs. Scaling S to 1 recovers the equations derived by Proctor & Weiss (1990) for case T in the limit of tall, thin rolls.

It is possible to let ζ be a second small parameter; this yields the same equations (17) as when the limits are taken in the opposite order.

In case T, equations (16) have chaotic solutions associated with a heteroclinic connection between a pair of saddle-foci satisfying Shil'nikov's criterion (Knobloch,

Proctor & Weiss 1991). Equations (16) are more complicated in case H ($\gamma \neq 0$) than in case T, as there is an extra nonlinearity in the first equation. I am not aware of the more complicated version having been analysed in the literature, but the analysis is of limited interest, as equations (16) are not an asymptotically exact model of the full PDEs. Equations (17) also have chaotic solutions associated with a heteroclinic connection between a pair of saddle-foci satisfying Shil'nikov's criterion (Proctor & Weiss 1990).

3.3. Cases V and R

Here, the situation is somewhat more complicated, as there are two geometrical limits that introduce small parameters: tall, thin rolls ($\varpi \to 0$) and short, wide rolls ($\delta \to 0$). In the limit of small diffusivity, we obtain by a similar derivation a set of equations equivalent to equations (16); if we consider the limit of short wide rolls (with or without small diffusivity), we obtain equations equivalent to equations (17). These situations are of limited interest, as it is unrealistic to expect convection to occur in short, wide rolls: these will always be unstable to narrower rolls.

The more interesting geometrical limit is the limit of tall, thin rolls. Here ϖ is the small parameter, and ζ is not taken to be small, since this does not introduce a relevant small parameter. The appropriate scaling is

$$a = \varpi m, \qquad b = \varpi n, \qquad c = \varpi^2 p, \qquad d = \varpi q, \qquad e = \varpi^2 r,$$

with time scaled by a factor of $1/\varpi$ from the original time. The variables n, q and r may be eliminated in favour of m and p by a series of substitutions, given here in more detail. The equations (12) for $\dot{n}$, $\dot{q}$ and $\dot{r}$ are rearranged:

$$\begin{aligned} n &= m - \varpi\dot{n} - \varpi^2 mp, \\ q &= m/\zeta - \varpi\dot{q}/\zeta - \varpi^2 mr/\zeta, \\ r &= \varpi r/4 - \varpi\dot{r}/4\zeta + \varpi mq/4\zeta, \end{aligned}$$

and substituted back into themselves several times to give

$$\begin{aligned} n &= m - \varpi\dot{m} + \varpi^2(\ddot{m} - mp) + \mathcal{O}(\varpi^3), \\ q &= m/\zeta - \varpi\dot{m}/\zeta^2 + \varpi^2\ddot{m}/\zeta^3 + \mathcal{O}(\varpi^3), \\ r &= \varpi m^2/4\zeta^2 + \varpi^2(\zeta m^2 - 6m\dot{m})/16\zeta^3 + \mathcal{O}(\varpi^3). \end{aligned}$$

These expressions are substituted into the equations for $\dot{m}$ and $\dot{p}$ to give two equations:

$$\begin{aligned} 0 &= \varpi m(\text{linear combination of } \mu \text{ and } \nu) \\ &\qquad + \varpi^2\dot{m}(\text{linear combination of } \mu \text{ and } \nu) + \mathcal{O}(\varpi^3), \\ \varpi^3\dot{p} &= \varpi^3(-p + m^2) + \mathcal{O}(\varpi^4). \end{aligned}$$

The two leading order terms in the first equation may be brought to order ϖ^3 by rewriting μ and ν as

$$\mu = \varpi \frac{\Delta}{\sigma+\zeta}\kappa - \varpi^2 \frac{\Delta}{\zeta(\sigma+\zeta)}\lambda, \qquad \nu = \varpi \frac{\Delta}{\zeta(1+\sigma)}\kappa - \varpi^2 \frac{\Delta}{\zeta(1+\sigma)}\lambda.$$

By writing this, we are restricting μ and ν to a narrow range of permissible parameter values; outside this parameter régime, we will get at most a first-order ODE. The equations resulting from bringing the order ϖ and ϖ^2 terms to order ϖ^3 are:

$$\ddot{m} + \lambda m = \kappa \dot{m} - Smp,$$
$$\dot{p} = -p + m^2,$$

where

$$S = \begin{cases} \dfrac{\zeta(\sigma+\zeta)}{\Delta(1-\zeta)} & \text{case V,} \\ \dfrac{2\sigma^2}{(1+2\sigma)(1-\sigma)} & \text{case R.} \end{cases}$$

By rescaling m and p:

$$m = S^{-\frac{1}{2}} v, \qquad p = S^{-1} w,$$

the equations are brought into a convenient form, with all inessential constants removed:

$$\begin{aligned} \ddot{v} + \lambda v &= \kappa \dot{v} - vw, \\ \dot{w} &= -w + v^2. \end{aligned} \tag{19}$$

Since conditions (13)–(14) are satisfied, equations (19) are an asymptotically exact approximation to the full PDEs. They are equivalent to a set of equations put forward by Shimizu & Morioka (1980) as an *ad hoc* model of the Lorenz equations in the limit of large Rayleigh number; Shimizu and Morioka considered only very large negative values of λ; here we are concerned with order 1 values of λ. Although equations (19) differ from equations (17) only in the sign of the nonlinearity in the first equation, the nonlinear solutions are qualitatively very different: the chaos found in equations (19) is associated with a homoclinic connection to a saddle (the same mechanism that operates in the Lorenz equations) rather than with a heteroclinic connection between a pair of saddle-foci.

4. Dynamics of the model equations

Equations (19) can be expressed as a set of three coupled ODEs:

$$\begin{aligned} \dot{u} &= \kappa u - \lambda v - vw, \\ \dot{v} &= u, \\ \dot{w} &= -w + v^2. \end{aligned} \tag{20}$$

The equations are symmetric under the substitution $(u, v, w) \to (-u, -v, w)$; this is a manifestation of the invariance of the PDEs under inversion of the sense of the flow. The divergence of the equations is $\kappa - 1$, so the system is dissipative if $\kappa < 1$, a condition necessary for the existence of an attractor. The trivial solution $u = v = w = 0$ undergoes a subcritical Hopf (oscillatory) bifurcation at $\kappa = 0$ with $\lambda \geq 0$; the steady solutions $(0, \pm\sqrt{-\lambda}, -\lambda)$ are created in a pitchfork bifurcation at $\lambda = 0$, and undergo a supercritical Hopf bifurcation at $\lambda = \frac{1}{2}\kappa(1 - \kappa)$ with $\kappa \leq 0$.

We will use the notation of Sparrow (1982) and describe periodic orbits of equations (20) by symbol sequences of x's and y's, indicating how the orbit loops around the right ($v > 0$) or the left ($v < 0$) equilibrium points; asymmetric orbits will be prefixed with an A unless there is an odd number of symbols in the sequence (in which case the orbit is bound to be asymmetric). Bifurcations will be prefixed with the simplest orbit involved in the bifurcation, so, for example, the Hopf bifurcation from the steady equilibrium points, at which the x-orbits are created, is the x-Hopf bifurcation.

In order to present solutions to equations (20), we will hold the parameter Q (the Chandrasekhar number or the Taylor number) fixed while increasing the Rayleigh number R. This corresponds to considering a line through the (κ, λ) plane with increasing κ and decreasing λ. If Q is above its critical value, then the bifurcation diagram is as shown in Figure 2(c). The first bifurcation as κ increases is a subcritical Hopf bifurcation; beyond this point, all trajectories escape to infinity, so in this parameter régime, the model does not capture the behaviour of the full system.

If Q is below its critical value, then the bifurcation diagram is as in Figure 3 (Arnol'd 1977). The first bifurcation as κ increases is a supercritical pitchfork bifurcation, in which symmetric steady solutions are created. These solutions lose their stability in the supercritical x-Hopf bifurcation, which gives rise to a symmetric pair of periodic orbits circling the non-stable steady solutions (the x-orbits – Figure 4(a)). As κ continues to increase, these periodic orbits increase in size until they "glue" together in a double homoclinic connection to the trivial solution (Figure 4(b)). In this "gluing" bifurcation (Coullet, Gambaudo & Tresser 1984), the two asymmetric periodic orbits are destroyed and replaced by a single symmetric periodic orbit (the xy-orbit – Figure 4(c)). This xy-orbit continues to grow until either it is destroyed in an xy-saddle-node (xy-SN) bifurcation with a larger non-stable xy-orbit, or it escapes to infinity. Beyond this point (not shown), all trajectories are unbounded, so the model no longer captures the behaviour of the full system.

It is interesting to compare the bifurcation diagram for vertical magnetoconvection in tall, thin rolls (Figure 3) with bifurcation diagrams for other double convection problems. Figure 5 shows the results of Knobloch & Proctor (1981) for the case of vertical magnetoconvection in rolls with aspect ratio of order 1: the bifurcation to oscillatory convection is supercritical, but the bifurcation to steady convection may be supercritical or subcritical. The analysis of the transitions between these

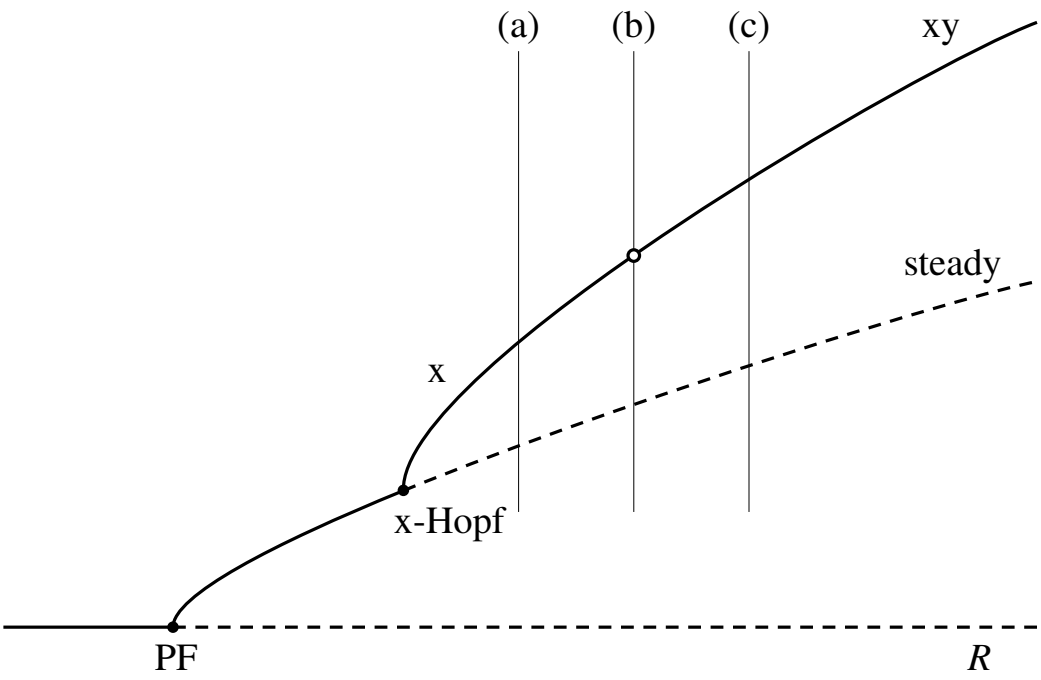

Figure 3. *Schematic bifurcation diagram for vertical magnetoconvection or convection in a rotating layer in tall, thin rolls, assuming that Q is below its critical value. This and subsequent bifurcation diagrams have R or κ on the horizontal axis, and the amplitude of the solution on the vertical axis. Stable and non-stable solutions are represented by solid and dashed lines respectively. Filled circles represent local (pitchfork (PF), saddle-node (SN) or Hopf) bifurcations; open circles represent global (homoclinic or heteroclinic) bifurcations. In this diagram, which is a bifurcation diagram of equations (15) with $M < 0$ and $N > 0$, the open circle represents an x-gluing bifurcation. The vertical lines labelled (a), (b) and (c) represent the parameter values used in computing the orbits shown in Figure 4.*

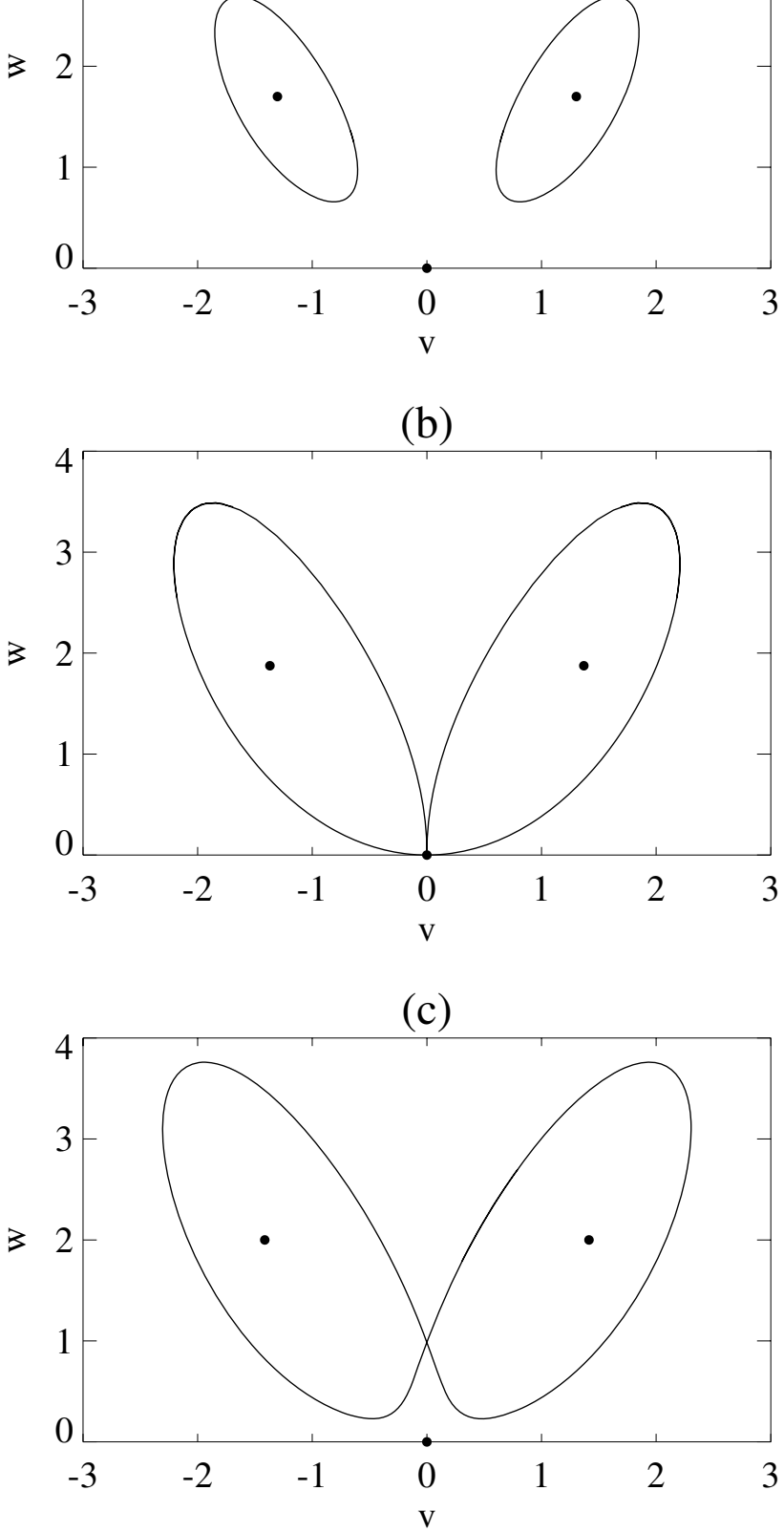

Figure 4. *Typical solutions of equations (20) at the parameter values indicated in Figure 3: (a) a pair of x-orbits; (b) the x-gluing bifurcation; (c) an xy-orbit. The filled circles represent the three steady solutions. Note that these are projections onto the (v, w) plane: the xy-orbit in (c) does not actually intersect itself.*

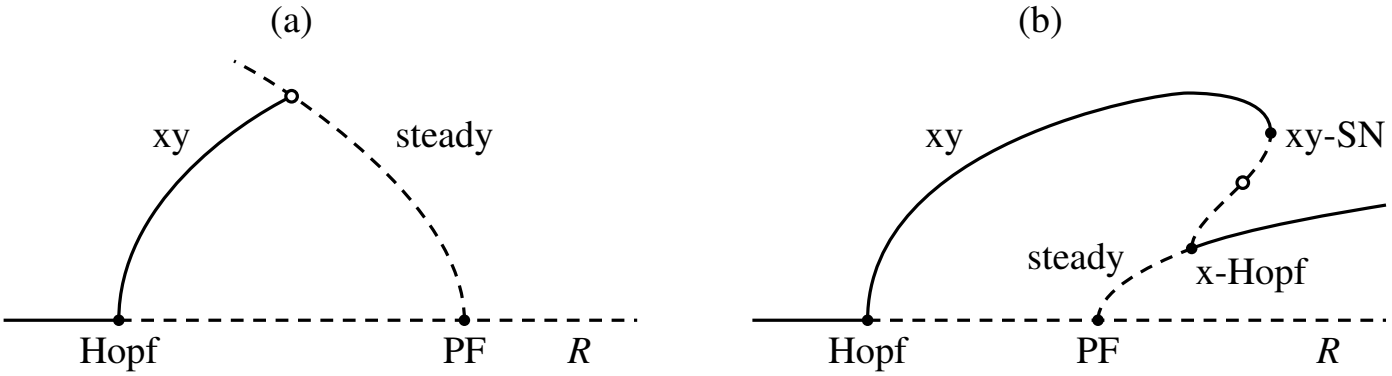

Figure 5. *Schematic bifurcation diagrams for vertical magnetoconvection in the limit of small amplitude in rolls with order 1 aspect ratio, with Q greater than its critical value (after Knobloch & Proctor 1981). The Hopf bifurcation to oscillatory convection is supercritical, while the pitchfork (PF) bifurcation to steady convection is subcritical in (a), supercritical in (b). The open circles represent global bifurcations: a heteroclinic bifurcation in (a) and a gluing bifurcation in (b). Other symbols and abbreviations are defined in the caption to Figure 3. The two diagrams here are bifurcation diagrams of equations (15) with (a) $M > 0$, $N < 0$; (b) $M < 0$, $N < 0$.*

various bifurcation diagrams as the aspect ratio and the Prandtl number are varied would involve studying bifurcations of higher codimension – see, for example, Dangelmayr, Armbruster & Neveling (1985). Figure 5(a) also describes thermosolutal convection (Da Costa *et al.* 1981) and convection in a rotating layer (Guckenheimer & Knobloch 1983), and Figure 5(a) and (b) describe horizontal magnetoconvection in narrow and wide rolls respectively (Arter 1983).

A key parameter in the analysis of equations (20) is the saddle index δ, the absolute value of the ratio of the negative eigenvalue nearest zero to the positive eigenvalue of the trivial solution. If we focus our attention on the gluing bifurcation, a necessary condition for the homoclinic orbits to be stable is that δ be greater than one: contraction must be stronger than expansion (Guckenheimer & Holmes 1986). This condition is satisfied if $\lambda > \kappa - 1$, in region I of Figure 6.

Tracking the gluing bifurcation numerically (Figure 6) shows that it enters region II at the point B ($(\kappa, \lambda) \approx (-1.724, -2.724)$). In region II, where $\delta < 1$, all orbits involved in homoclinic connections to the trivial solution must be unstable. The point B is a codimension-two homoclinic bifurcation point; an analysis near this point (Lyubimov & Zaks 1983; Rucklidge 1991) reveals that the x-gluing bifurcation in region I splits into a more complicated sequence of bifurcations as it enters region II. This sequence of bifurcations (illustrated in Figure 7) has the same net effect as the x-gluing bifurcation. The stable x-orbit becomes unstable in an x-saddle-node (x-SN) bifurcation and is destroyed in the x-homoclinic bifurcation. An unstable xy-orbit is created in the x-homoclinic bifurcation; it gains stability in a subcritical xy-symmetry breaking (xy-SB) bifurcation and emerges on the right of

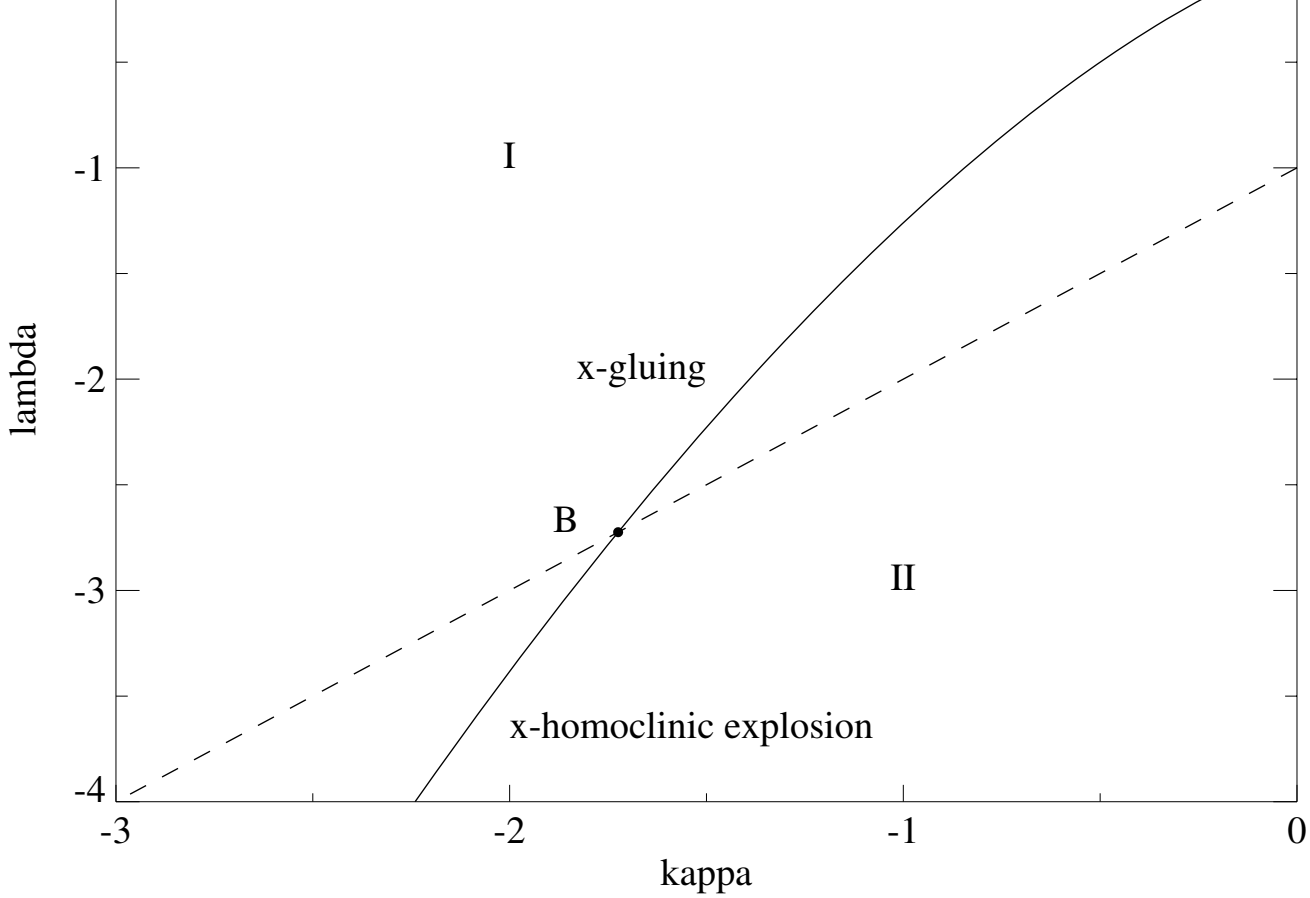

Figure 6. *Numerically computed location of the x-homoclinic bifurcation (solid line). The dashed line indicates where $\delta = 1$. In region I, where $\delta > 1$, the homoclinic bifurcation is an x-gluing bifurcation, while in region II, $\delta < 1$, and we have an x-homoclinic explosion: there will be chaotic trajectories to the right of the solid line, in a wedge below the point B.*

the figure. The unstable Axy-orbit created in the xy-symmetry breaking bifurcation is destroyed in the Axy-homoclinic bifurcation.

The x- and Axy-homoclinic bifurcations are in fact homoclinic explosions (Sparrow 1982), which give rise to a strange invariant set: an infinite number of unstable periodic and aperiodic trajectories. Between the two homoclinic explosions is a parameter interval in which the strange invariant set is attracting. In this parameter interval, there are chaotic trajectories, which never repeat themselves and have sensitive dependence on initial conditions: two trajectories started arbitrarily close together will eventually diverge and evolve independently. A typical trajectory from this chaotic interval in shown in Figure 8(a): it looks similar to the homoclinic orbits shown in Figure 4(b), but an examination of the trajectory near the trivial solution in Figure 8(b) reveals that it is chaotic.

At this point, we have established the existence of chaos in these ODEs (20) in a wedge of parameter space below the point B. These chaotic trajectories are mild – the amplitude does not vary greatly between oscillations; it is only the sense of the

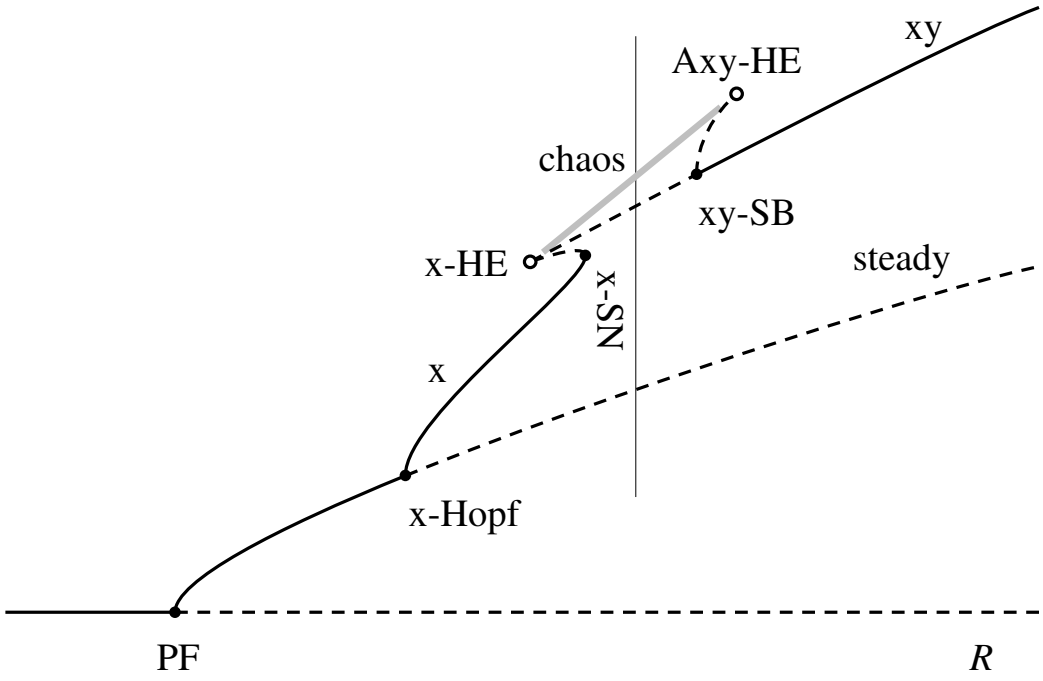

Figure 7. *Schematic bifurcation diagram in region II. The x-gluing bifurcation has split into an x-homoclinic explosion (x-HE) and an Axy-homoclinic implosion (Axy-HE). The strange attractor is represented by the shaded band between the global bifurcations. Two periodic orbits created in the x-homoclinic explosion persist outside the interval between the global bifurcations: a pair of unstable x-orbits turn around in the x-saddle-node (x-SN) bifurcation and emerge on the left as stable periodic orbits, and an unstable xy-orbit gains stability in an xy-symmetry breaking (xy-SB) bifurcation and emerges on the right. The unlabelled vertical line represents the parameter value used in computing the trajectory shown in Figure 8.*

overturning convective motion that is unpredictable. However, the equations (20), like the Lorenz equations, are capable of more exotic behaviour – see Figure 9 – for parameter values that are still order 1. It is the aim of the remainder of this section to present a brief analysis of the equations. The reader is referred to Rucklidge (1991) and to Shil'nikov (1986 and 1989) for more details.

The four new bifurcations depicted in Figure 7 begin at the point B where the x-gluing bifurcation crosses into region II of Figure 6. These bifurcations are followed numerically using the continuation package AUTO (Doedel 1986); the results are shown schematically in Figure 10, which includes the principal bifurcation lines and attracting sets. Emerging from the point B are the four bifurcation lines: the x-homoclinic explosion (x-HE) and the x-saddle-node bifurcation lines continue towards more negative values of λ, while the xy-symmetry breaking bifurcation and the Axy-homoclinic explosion (Axy-HE) loop back towards smaller values of λ before turning around again.

At the point E, the xy-symmetry breaking bifurcation becomes supercritical

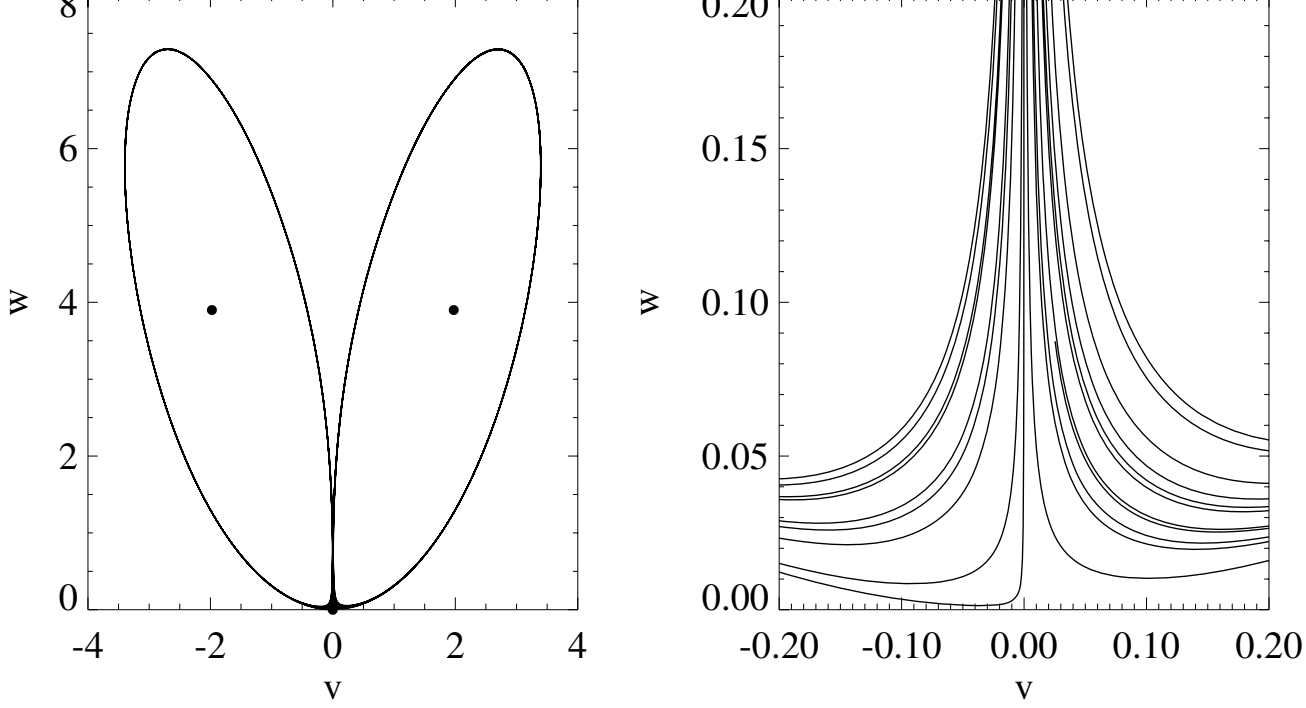

Figure 8. *Typical chaotic trajectory at the parameter values from Figure 7:* $(\kappa, \lambda) = (-2.2, -3.9)$. *(a) The entire trajectory; (b) detail near the trivial solution. The filled circles in (a) represent the three steady solutions.*

by emitting a line of Axy-saddle-node (Axy-SN) bifurcations. This line terminates at the point D, where it connects to the Axy-homoclinic explosion line. An analysis of the point D (Rucklidge 1991) reveals the structure illustrated in the figure: four bifurcation lines enter D from above and four more leave D from below. It is here that the first period-doubling bifurcation is created: the Axy-orbit bifurcates an unstable Axyxy-orbit at the subcritical Axy-period doubling (Axy-PD) bifurcation. This bifurcation becomes supercritical as λ decreases below the point D. The process of creation of period-doubling bifurcations continues; numerical experiments reveal that for λ less than about -6, there is a complete period-doubling cascade as κ decreases from -1, with the chaotic trajectories and periodic windows familiar from the logistic map (May 1976).

Thus we have shown that the ODEs (20) have chaotic trajectories created in two different manners: either in a homoclinic explosion, with an abrupt transition to chaos; or in a period-doubling cascade, with a more gradual transition to chaos. Further analysis reveals the existence of more complicated codimension-two bifurcation points involving heteroclinic connections between the trivial solution and the two nontrivial equilibrium points (Glendinning & Sparrow 1986). A line of Shil'nikov bifurcations (homoclinic connections to a saddle-focus) emerges from this point; associated with it are period-doubling cascades and chaotic trajectories interspersed with periodic windows.

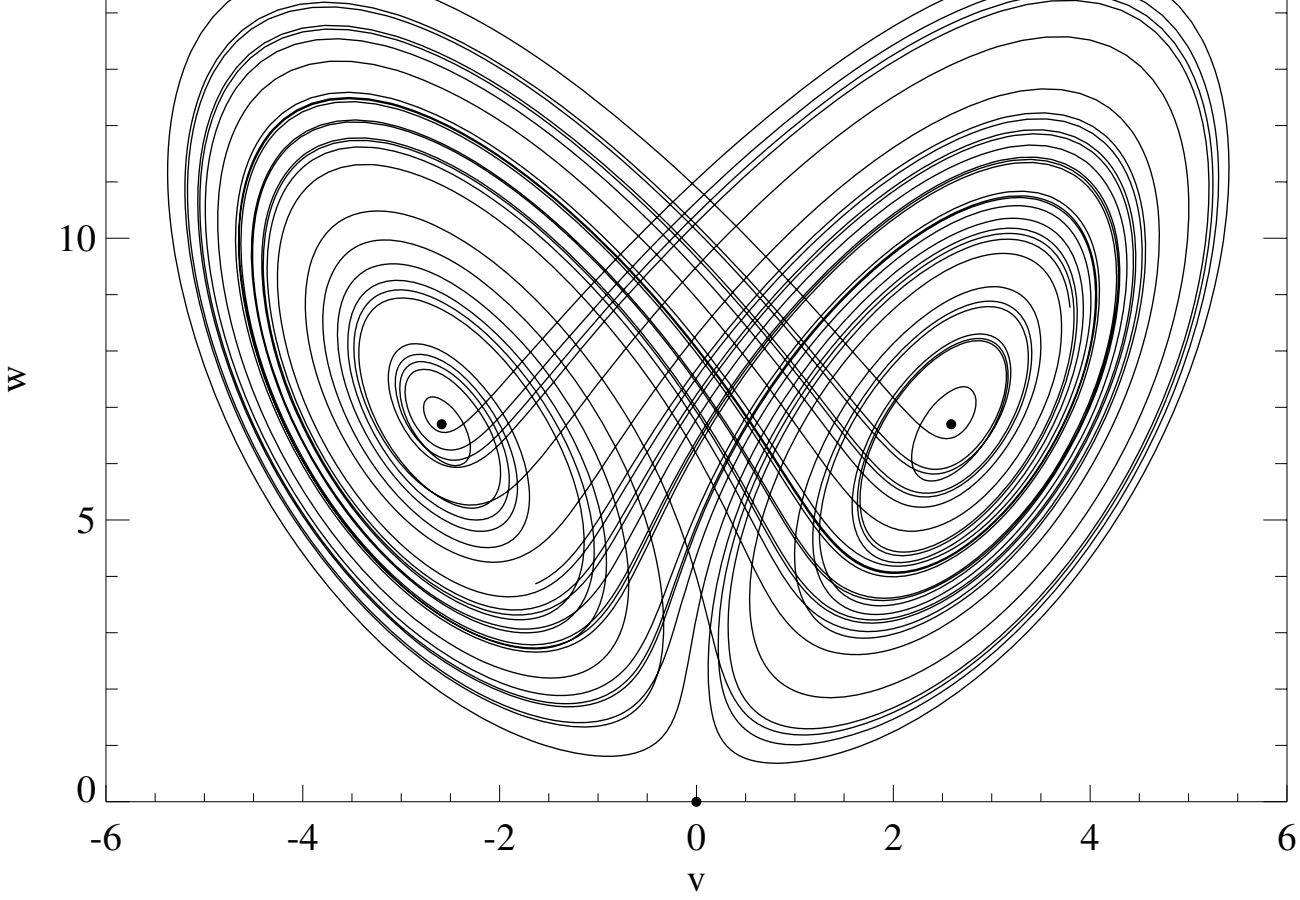

Figure 9. *Typical chaotic trajectory of equations (20), for* $(\kappa, \lambda) = (-2.0, -6.7)$.

5. Discussion

The various limits in which we can derive ODEs that give asymptotically exact descriptions of the PDEs (5)–(8) near the point C have been presented. The limit of small amplitude yields the second-order ODEs (15); if we introduce a small parameter by considering the limit of tall, thin rolls, we obtain third or higher order ODEs: (17), (18) and (20). The limit $\zeta \to 0$ does not give asymptotically exact equations unless the amplitude is small, in which case we recover the second-order ODEs (15). The limit of short, wide rolls in cases V and R yields the asymptotically exact ODEs (17), but in these cases, we would expect the wide rolls to break up into narrower rolls.

The existence of chaotic solutions in the asymptotically exact ODEs implies the existence of chaotic solutions in the corresponding set of PDEs, in the asymptotic limit. This is a significant result, as it provides an insight into the nature of the chaos that has been observed numerically in the PDEs, and predicts parameter régimes where one should expect to find chaotic trajectories. Equations (17) have chaotic solutions associated with a Shil'nikov bifurcation (Proctor & Weiss 1990); their results applied to case H demonstrate that the PDEs for magnetoconvection have chaotic solutions. Moreover, we have shown that equations (20) have Lorenz-

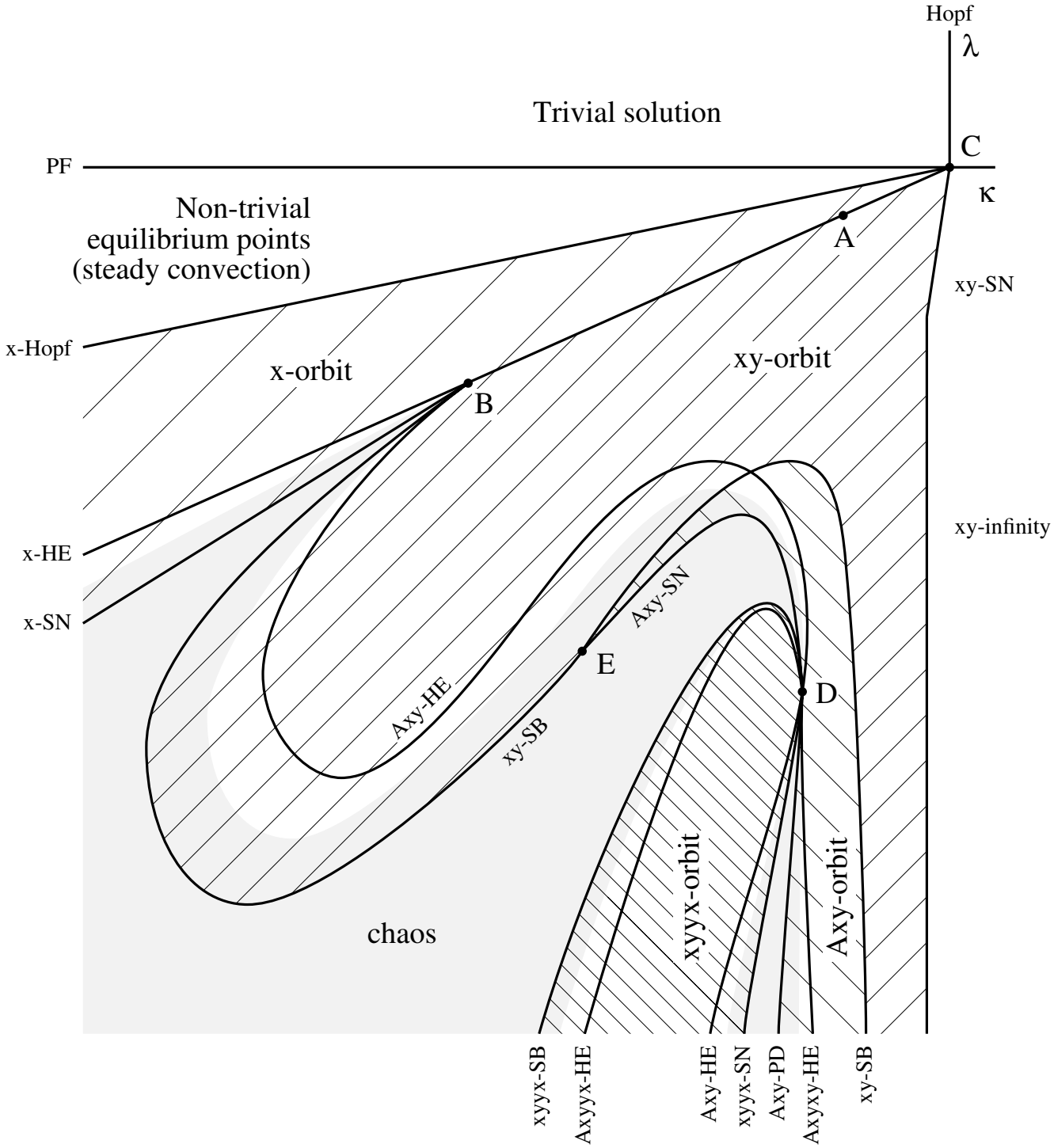

Figure 10. *Schematic unfolding diagram of equations (20), showing the principal bifurcation lines and attracting sets (after Rucklidge 1991). The domains of stability of the four simplest periodic orbits are shown as hatched regions: the x- and xy-orbits are singly and doubly hatched, slanting upwards to the right, and the Axy- and xyxy-orbits are doubly and quadruply hatched, slanting downwards to the right. The regions with attracting chaotic trajectories are shown as tinted grey.*

like chaotic trajectories, which establishes the existence of chaos in the PDEs for convection in an imposed vertical magnetic field and in a rotating layer, in the limit of tall, thin rolls. Such chaotic solutions have not yet been found in the PDEs (Weiss 1981a and 1981b), but this work suggests the parameter régimes that might bear fruit; numerical studies of the PDEs for convection in a vertical magnetic field are in progress.

In the situations studied in detail in this paper (cases V and R in the limit of tall, thin rolls), the linear theory predicts that if Q is greater than its critical value, there is an initial bifurcation to oscillatory convection. The subcritical oscillatory solutions are unstable and do not turn around and become stable; higher order corrections to the model equations could achieve this (Rucklidge, Weiss, Brownjohn & Proctor 1991). If Q is less than its critical value, the supercritical pitchfork bifurcation is followed immediately by a supercritical Hopf bifurcation. Indeed, it is in the parameter régime where the linear theory does not predict oscillatory convection that we find chaotic trajectories. This reflects the essentially nonlinear nature of convection.

By considering the codimension-two point C in these particular limiting situations, we have in effect increased the codimension of the principal bifurcation point. The advantage of doing this is that bifurcation points act as organising centres: the low-order models are exact only in an asymptotically small (but finite) neighbourhood of the bifurcation point but, in practice, such models are found to be reliable guides to the behaviour of the full system in a region of parameter space that grows with the codimension of the bifurcation point. It is essential to have reliable low-order models if we are to understand the nature of complicated behaviour observed in the PDEs. Moreover, using low-order models, it is possible to perform detailed numerical experiments that would be impossible with the full PDEs.

It is important to discuss the extent to which the mathematical idealisations made in deriving these model ODEs affect the physical relevance of the results. We have assumed that there are no instabilities to higher order spatial structures; this is clearly not true in cases V and R in the limit of short, wide rolls, as the preferred aspect ratio is for tall, thin rolls. It is true for all the other cases discussed: the tall thin box that we require for the analysis is narrower than the preferred aspect ratio. Moreover, the Rayleigh numbers we are considering are just above critical, where we would expect a simple spatial structure, so the idealised flows that we have been considering are realisable in principle.

The other two-dimensional instability that must be considered is that of travelling convective rolls. Travelling waves are always prevented by the side walls of the box; they become possible if we use periodic instead of stress-free side boundary conditions. In this case, whether stationary rolls are unstable to travelling rolls depends on a fine balance between higher order nonlinear terms. In cases T and H, travelling rolls are preferred (Knobloch 1986a and 1986b). In case V, stationary rolls are preferred near the codimension-two point C (Dangelmayr & Knobloch 1986).

In case R, stationary rolls are preferred if σ is small enough (Knobloch & Silber 1990).

In practice, the two-dimensional flows that we have considered may be unstable to three-dimensional disturbances, but in several instances, such as convection in a strong vertical magnetic field or convection in a rapidly rotating layer, tall, thin rolls are the preferred form of motion. In case V, we require $\zeta < 1$ for the existence of the codimension-two point C; this is not attainable in the laboratory, but is of astrophysical relevance. In case R, we require $\sigma < 1$ for the same reason; this condition is satisfied by, for example, mercury. It is in this situation that the chaotic convection predicted by the low order models may be experimentally accessible. To date, experimental observations of double convection have concentrated on binary convection and thermosolutal convection in large aspect ratio systems, rather than the narrow boxes that we require, so chaotic solutions of the type described in this paper have not been observed.

I wish to express my gratitude to Nigel Weiss, under whose supervision and encouragement this work was carried out. I also want to thank Keith Julien, Edgar Knobloch and Mike Proctor for many stimulating discussions, and Paul Matthews, Emily Stone and Beverley White for their helpful suggestions on a first draft of this paper. This work was supported by the Commonwealth Scholarship and Fellowship Plan and by Trinity College, Cambridge.

References

Arnéodo, A., Coullet, P.H. & Spiegel, E.A. 1982 Chaos in a finite macroscopic system. *Phys. Lett. A* **92**, 369–373.

Arnéodo, A., Coullet, P.H. & Spiegel, E.A. 1985 The dynamics of triple convection. *Geophys. Astrophys. Fluid Dynamics* **31**, 1–48.

Arnéodo, A. & Thual, O. 1985 Direct numerical simulations of a triple convection problem versus normal form predictions. *Phys. Lett. A* **109**, 367–373.

Arnol'd, V.I. 1977 Loss of stability of self-oscillations close to resonance and versal deformations of equivariant vector fields. (in Russian) *Funct. Anal. Applic.* **11**, 1–10.

Arter, W. 1983 Nonlinear convection in an imposed horizontal magnetic field. *Geophys. Astrophys. Fluid Dynamics* **25**, 259–292.

9479–524

Coullet, P.H. & Spiegel, E.A. 1983 Amplitude equations for systems with competing instabilities. *SIAM J. Appl. Math.* **43**, 776–821.

Coullet, P., Gambaudo, J.-M. & Tresser, C. 1984 Une nouvelle bifurcation de codimension 2: le collage de cycles. *C. R. Acad. Sc. Paris* **299**, Série I, 253–256.

Curry, J.H., Herring, J.R., Loncaric, J. & Orszag, S.A. 1984 Order and disorder in two- and three-dimensional Bénard convection. *J. Fluid Mech.* **147**, 1–38.

Da Costa, L.N., Knobloch, E. & Weiss, N.O. 1981 Oscillations in double-diffusive convection. *J. Fluid Mech.* **109**, 25–43.

Dangelmayr, G., Armbruster, D. & Neveling, M. 1985 A codimension three bifurcation for the laser with saturable absorber. *Z. Phys. B – Condensed Matter* **59**, 365–370.

Dangelmayr, G. & Knobloch, E. 1986 Interaction between standing and travelling waves and steady states in magnetoconvection. *Phys. Lett. A* **117**, 394–398.

Deane, A.E. & Sirovich, L. 1991 A computational study of Rayleigh–Bénard convection. Part 1. Rayleigh-number scaling. *J. Fluid Mech.* **222**, 231–250.

Doedel, E. & Kernévez, J. 1986 *AUTO: Software for Continuation and Bifurcation Problems in Ordinary Differential Equations.* CalTech Press: Pasadena.

Glendinning, P. & Sparrow, C. 1984 Local and global behaviour near homoclinic orbits. *J. Stat. Phys.* **35**, 645–696.

Glendinning, P. & Sparrow, C. 1986 T-points: a codimension two heteroclinic bifurcation. *J. Stat. Phys.* **43**, 479–488.

Guckenheimer, J. & Knobloch, E. 1983 Nonlinear convection in a rotating layer: amplitude expansions and normal forms. *Geophys. Astrophys. Fluid Dynamics* **23**, 247–272.

Guckenheimer, J. & Holmes, P. 1983 *Nonlinear Oscillations, Dynamical Systems and Bifurcations of Vector Fields.* Springer: New York.

Huppert, H.E. & Moore, D.R. 1976 Nonlinear double-diffusive convection. *J. Fluid Mech.* **78**, 821–854.

Knobloch, E. 1986a On convection in a horizontal magnetic field with periodic boundary conditions. *Geophys. Astrophys. Fluid Dynamics* **36**, 161–177.

Knobloch, E. 1986b On the degenerate Hopf bifurcation with $O(2)$ symmetry. *Contemp. Math.* **56**, 193–201.

Knobloch, E. & Proctor, M.R.E. 1981 Nonlinear periodic convection in double-diffusive systems. *J. Fluid Mech.* **108**, 291–316.

Knobloch, E. & Silber, M. 1990 Travelling wave convection in a rotating layer. *Geophys. Astrophys. Fluid Dynamics* **51**, 195–209.

Knobloch, E., Weiss, N.O. & Da Costa, L.N. 1981 Oscillatory and steady convection in a magnetic field. *J. Fluid Mech.* **113**, 153–186.

Knobloch, E., Moore, D.R., Toomre, J. & Weiss, N.O. 1986 Transitions to chaos in two-dimensional double-diffusive convection. *J. Fluid Mech.* **166**, 409–448.

Knobloch, E., Proctor, M.R.E. & Weiss, N.O. 1992 Heteroclinic bifurcations in a simple model of double-diffusive convection. *J. Fluid Mech.* **239**, 273–292.

Lorenz, E.N. 1963 Deterministic nonperiodic flow. *J. Atmos. Sci.* **20**, 130–141.

Lyubimov, D.V. & Zaks, M.A. 1983 Two mechanisms of the transition to chaos in finite-dimensional models of convection. *Physica* **9D**, 52–64.

May, R.M. 1976 Simple mathematical models with very complicated dynamics. *Nature* **261**, 459–467.

Moore, D.R. & Weiss, N.O. 1973 Two-dimensional Rayleigh–Bénard convection. *J. Fluid Mech.* **58**, 289–312.

Proctor, M.R.E. & Weiss, N.O. 1990 Normal forms and chaos in thermosolutal convection. *Nonlinearity* **3**, 619–637.

Rucklidge, A.M. 1993 Chaos in a low-order model of magnetoconvection. *Physica* **62D**, 323–337.

Rucklidge, A.M., Weiss, N.O., Brownjohn, D.P. & Proctor, M.R.E. 1993 Oscillations and secondary bifurcations in nonlinear magnetoconvection. *Geophys. Astrophys. Fluid Dynamics* **68**, 133–150.

Shil'nikov, A.L. 1986 Bifurcations and chaos in the Morioka–Shimizu system (in Russian), in *Methods of Qualitative Theory of Differential Equations*. Gorky State University, 180–193. Published in English (1991) *Selecta Math. Sov.* **10** 105–117.

Shil'nikov, A.L. 1989 Bifurcations and chaos in the Morioka–Shimizu model: II (in Russian), in *Methods of Qualitative Theory of Differential Equations and Theory of Bifurcations*. Gorky State University, 130–138.

Shil'nikov, L.P. 1965 A case of the existence of a countable number of periodic motions. *Soviet Math. Dokl.* **6**, 163–167.

Shimizu, T. & Morioka, N. 1980 On the bifurcation of a symmetric limit cycle to an asymmetric one in a simple model. *Phys. Lett. A* **76**, 201–204.

Sparrow, C. 1982 *The Lorenz Equations: Bifurcations, Chaos, and Strange Attractors*. Springer: New York.

Veronis, G. 1965 On finite amplitude instability in thermohaline convection. *J. Marine Res.* **23**, 1–17.

Veronis, G. 1966 Motions at subcritical values of the Rayleigh number in a rotating fluid. *J. Fluid Mech.* **24**, 545–554.

Weiss, N.O. 1981a Convection in an imposed magnetic field. Part 1. The development of nonlinear convection. *J. Fluid Mech.* **108**, 247–272.

Weiss, N.O. 1981b Convection in an imposed magnetic field. Part 2. The dynamical regime. *J. Fluid Mech.* **108**, 273–289.

Chaos in models of double convection

A.M. RUCKLIDGE

Department of Applied Mathematics and Theoretical Physics,
University of Cambridge, Cambridge CB3 9EW, UK

Abstract

In certain parameter régimes, it is possible to derive third-order sets of ordinary differential equations that are asymptotically exact descriptions of weakly nonlinear double convection and that exhibit chaotic behaviour. This paper presents a unified approach to deriving such models for two-dimensional convection in a horizontal layer of Boussinesq fluid with lateral constraints. Four situations are considered: thermosolutal convection, convection in an imposed vertical or horizontal magnetic field, and convection in a fluid layer rotating uniformly about a vertical axis. Thermosolutal convection and convection in an imposed horizontal magnetic field are shown here to be governed by the same sets of model equations, which exhibit the period-doubling cascades and chaotic solutions that are associated with the Shil'nikov bifurcation (Proctor & Weiss 1990). This establishes, for the first time, the existence of chaotic solutions of the equations governing two-dimensional magnetoconvection. Moreover, in the limit of tall, thin rolls, convection in an imposed vertical magnetic field and convection in a rotating fluid layer are both modelled by a new third-order set of ordinary differential equations, which is shown here to have chaotic solutions that are created in a homoclinic explosion, in the same manner as the chaotic solutions of the Lorenz equations. Unlike the Lorenz equations, however, this model provides an accurate description of convection in the parameter régime where the the chaotic solutions appear.

J. Fluid Mech. **237** 209–229 (1992).